Research Article | Vol. 28, No. 17 / 17 August 2020 / Optics Express 25335
Optics EXPRESS

Quantitative investigation of laser-induced damage fatigue in HfO_2 and ZrO_2 single layer coatings

LINAS SMALAKYS,* EVELINA DROBUŽAITĖ, BALYS MOMGAUDIS, ROBERTAS GRIGUTIS, AND ANDRIUS MELNINKAITIS

Laser Research Center, Vilnius University, Saulėtekio Ave. 10, LT-10223 Vilnius, Lithuania
linas.smalakys@ff.vu.lt

Abstract: The decrease of laser-induced damage threshold (LIDT) of optical materials when irradiated with multiple laser pulses is an important phenomenon commonly known as the optical fatigue effect. In case of pulsed femtosecond irradiation fatigue is usually attributed to incubation of laser-induced lattice defects. In this study, standard S-on-1 LIDT test was complimented with *in situ* time-resolved digital holographic microscopy (TRDHM) to quantitatively investigate fatigue of catastrophic damage for HfO_2 and ZrO_2 single layer ion-beam-sputtered optical coatings. It was identified that ablation (critical damage) was preceded by exponential increase in optical path length visible as positive phase shift (subcritical damage). Atomic force microscopy was used to show that physical damage originates as localized 100 nm wide nanogrooves perpendicular to laser polarization. A novel link was established between LIDT fatigue and mechanical fatigue crack growth from cyclic loads which allowed construction of a unified numerical fatigue model that reproduced both S-on-1 and TRDHM experimental data.

1. Introduction

The decrease of laser-induced damage threshold (LIDT) of optical materials when irradiated with multiple laser pulses, the so-called fatigue effect, is a well-known phenomenon inherent to almost all types of solids [1]. This effect is of major importance in high power laser applications as it limits the lifetime of critical laser components [2]. Fatigue effect can be readily observed by performing standardized S-on-1 test procedure [3] (where S stands for number of pulses) which measures probabilistic time to failure data at multiple irradiation fluence values. However, these tests are usually performed for a relatively small number of pulses (compared to real life applications) therefore predictive models are needed to extrapolate LIDT to higher number of pulses in order to estimate the expected lifetime of optical components.

In femtosecond regime fatigue was observed for various irradiation conditions [4] and is usually attributed to incubation of laser-induced or native intra-band gap states in the material [1,5,6] which leads to subsequent destabilization of lattice, nanocracking and subsequent catastrophic damage [7]. Presence of such defects was confirmed experimentally in bulk materials and coatings during the past few decades using various pump-probe techniques [5,8,9]. Accordingly, the current simplified picture of physics related to material degradation is as follows: an intense laser pulse non-linearly ionizes the material, conduction band electrons relax to self-trapped excitonic or other transient states, which are then converted to permanent defects or color centers [5]. Density of defects accumulates with subsequent laser pulses [10] and catastrophic damage occurs when critical density is reached [11]. Generic incubation models based on this picture were suggested and applied to a wide range of materials [12]. However, the exact nature of the incubation process or the critical density of such defects needed for predictive extrapolation models remains unknown.

#397812 https://doi.org/10.1364/OE.397812
Journal © 2020 Received 15 May 2020; revised 29 Jun 2020; accepted 5 Jul 2020; published 12 Aug 2020

Optics EXPRESS

In our recent study we have shown that multiple damage modes with different fatigue behaviours can exist on the same sample [13]. Therefore, the goal of this study is to investigate the fatigue of catastrophic laser-induced damage mode in greater detail with several experimental techniques. The aforementioned S-on-1 test was used to get the overall picture of the fatigue effect in selected single layer coatings, while time-resolved digital holographic microscopy (TRDHM) experiments were used for quantitative imaging of the irradiated area at selected fluence values.

2. Materials and methods

2.1. Single-layer coatings

Hafnia (HfO_2) and zirconia (ZrO_2) single-layer ion-beam-sputtered (IBS) coating samples were chosen for the fatigue studies. These are low absorption, high refractive index (bandgap is 5.6 and 5.3 eV respectively) dioxide materials used for coatings in the near-UV to IR spectral regions that can be used for applications which require high LIDT in the femtosecond regime [14]. Specifically, 25.4 mm diameter, 1 mm thickness fused silica substrates were coated with 2 QWOT at 1030 nm coatings (248 nm and 246 nm for hafnia and zirconia respectively) by ion-beam sputtering (IBS) for use in the experiments.

2.2. S-on-1 fatigue experiments

In order to extract the characteristic laser-induced damage fatigue curves for single layer dielectric coating samples, a modified S-on-1 damage threshold test was performed (schematic representation of experimental setup is provided in Fig. 1). Sample sites were irradiated with 10^n ($n = 0, 1, \ldots, 6$) number of pulses at the same fluence level, thus producing a grid in the fluence and number of pulses space. The irradiation was repeated for fluences with a fluence step of 0.015 J/cm^2 starting with the fluence below laser-induced damage threshold at specified number of pulses and finishing with the fluence above 1-on-1 damage threshold. Commercial femtosecond Yb:KGW laser (Pharos, Light Conversion) generating pulses at a central wavelength of 1030 nm and pulse duration of 304 fs (FWHM) with repetition rate of 50 kHz was used for irradiation. Laser beam was focused to 73.6 µm beam diameter (1/e^2) at the front surface of the samples. Both investigated samples were exposed at 45 deg. angle of incidence by using linear *s* polarization. *Ex situ* damage inspection was performed with differential interference contrast (DIC) microscope (BXFM, Olympus). LIDT of the catastrophic failure mode was evaluated for each pulse class separately as an average between the lowest damaged fluence level and the one below it to produce characteristic LIDT fatigue curves.

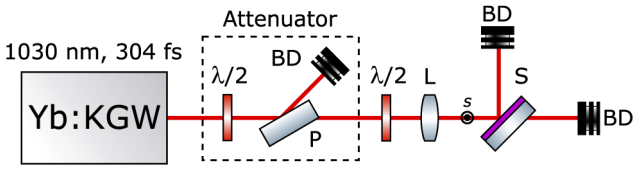

Fig. 1. Schematic representation of S-on-1 laser-induced damage setup: $\lambda/2$ – half-wave plate, P – thin film polarizer, BD – beam dump, L – focusing lens, S – sample, placed on a motorized stage.

2.3. TRDHM fatigue experiments

Even though S-on-1 experiments are commonly used for identifying fatigue and extrapolating LIDT to longer irradiations, they lack quantitative information about processes that precede catastrophic damage events. Therefore, additional *in situ* digital holographic microscopy experiments (schematic representation of experimental setup is provided in Fig. 2) were performed

Optics EXPRESS

on the single layer samples in order to investigate the irradiated coating area between laser pulses with 2D transmittance and phase shift resolution. Another Yb:KGW laser (Pharos, Light Conversion) was used to generate pump pulses of wavelength 1030 nm, pulse duration 380 fs (FWHM), beam diameter 43 μm at $1/e^2$ intensity level. Probe pulses were generated using in-house non-collinear optical parametric amplifier (NOPA) by pumping it with the third harmonic of the same laser. NOPA produced pulses with central wavelength of 529 nm and pulse duration of 30 fs (FWHM). Beam diameter of the probe pulses was more than 10 times larger than the pump's. Pumping was performed at 45 deg. angle of incidence while probing was performed from the rear (to avoid distortion of the phase front) at 0 deg. angle of incidence. Both pump and probe pulses had linear *s* polarization. During the experiment, digital holograms were recorded in single shot regime 1 second after the peak of the pump pulse using CCD camera (pixel size 3.45 μm). Such delay was chosen in order to avoid transient effects and detect only long-lived laser-induced changes that are relevant to the subsequent laser pulses. Digital holograms were reconstructed after the experiment using numerical convolution algorithm to retrieve relative transmittance and phase shift images. Regions of 5 x 5 μm were selected separately for each test site at highest phase shift areas and averaged to produce transmittance and phase shift signals.

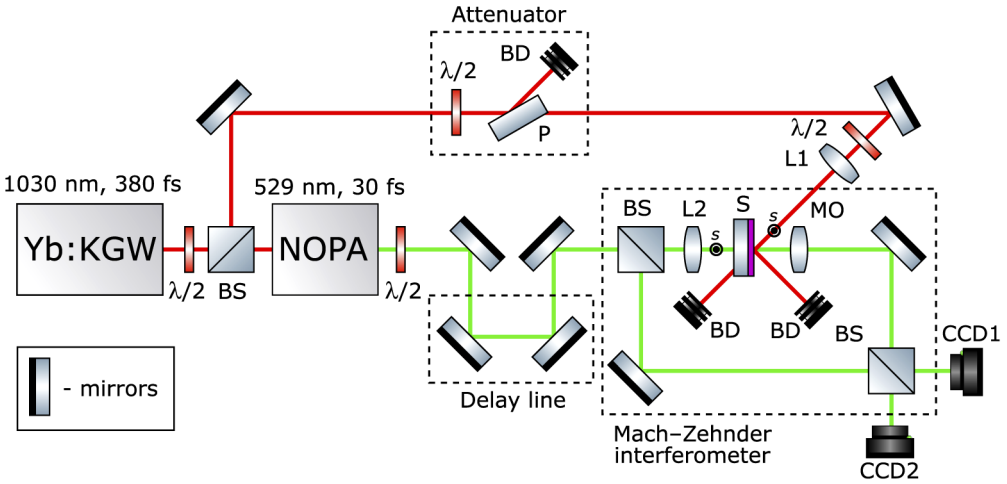

Fig. 2. Schematic representation of time-resolved digital holographic microscopy (TRDHM) experiment setup: $\lambda/2$ – half-wave plate, BS – beam splitter, P – thin film polarizer, BD – beam dump, L1, L2 – focusing lenses, MO – microscope objective, CCD1, CCD2 – digital CCD cameras, S – sample, placed on a motorized stage.

Four fluence levels between 1-on-1 and 250-on-1 LIDT were selected empirically for each coating (see Fig. 3). At each fluence level 15 test sites were irradiated with up to 250 laser pulses at 0.5 Hz repetition rate while recording digital hologram between each pulse. Repetition rate was limited by the acquisition speed of the holographic imaging system. Irradiation was stopped after catastrophic damage of the coating occurred to prevent contamination of nearby sites with ablation products.

2.4. *Observation of subcritical damage morphologies*

Since TRDHM fatigue experiment described in the previous section was performed until catastrophic damage became apparent, all traces of damage precursor morphologies were removed due to ablation. Therefore, additional experiment was performed at several test sites by reconstructing holograms *in situ* between laser pulses at 0.5 Hz and manually stopping irradiation after changes in transmittance and phase shift were detected (just before the critical damage

Optics EXPRESS

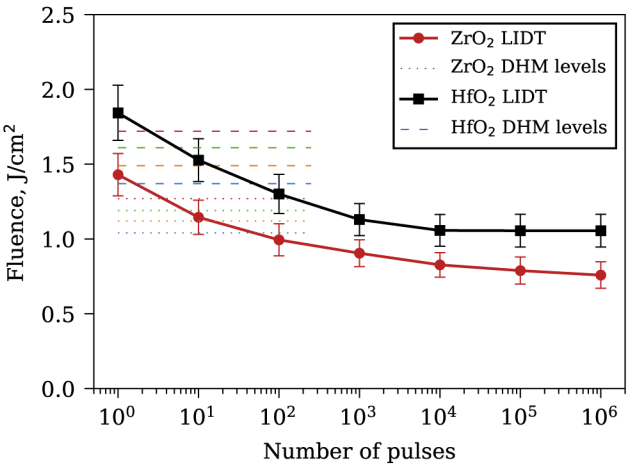

Fig. 3. Characteristic S-on-1 catastrophic damage fatigue curves for HfO_2 and ZrO_2 single layers coatings. Irradiation conditions: wavelength – 1030 nm, pulse duration – 304 fs, beam diameter ($1/e^2$) – 73.6 μm, repetition rate – 50 kHz.

has occurred). Irradiated sites were inspected afterwards using differential interference contrast microscope (BXFM, Olympus) and atomic force microscope (Dimension Edge, Veeco) in order to identify the nature of catastrophic damage precursors.

3. Results and discussion

3.1. S-on-1 damage test

Characteristic damage curves for catastrophic failure mode of HfO_2 and ZrO_2 coatings are provided in Fig. 3. HfO_2 exhibited higher LIDT at all tested pulse numbers. Fatigue effect is evident for both coatings: HfO_2 LIDT decreased from 1.84 J/cm^2 at single pulse irradiation to 1.05 J/cm^2 at 10^6 pulse irradiation while ZrO_2 LIDT decreased from 1.43 J/cm^2 at single pulse irradiation to 0.76 J/cm^2 at 10^6 pulse irradiation. LIDT appears to reach fatigue limit after around 10^4 pulses for both coatings. It is important to once again note that these damage curves were obtained for catastrophic damage only. ZrO_2 exhibited additional damage mode (laser-induced color change) which was studied in our previous study [13].

3.2. Investigation of fatigue with TRDHM

S-on-1 fatigue curves were used to select four fluence levels at equal intervals in the highest slope range for each coating at which TRDHM fatigue experiments were performed (dotted and dashed lines in Fig. 3 for zirconia and hafnia respectively). Survival functions for critical damage, estimated using Kaplan–Meier method [15], are provided in Fig. 4. Not all test sites were damaged after irradiation with 250 laser pulses at the lowest fluence levels. It is evident that multiple pulse critical damage is a stochastic, defect-driven process since deterministic process would have produced step-like survival functions.

Several stages of laser-induced damage initiation were observed at all investigated fluence levels during irradiation. Typical cases for both coatings are provided in Fig. 5. Localized changes mostly in phase shift (subcritical damage) were observed near the center of the beam (areas P1 and P2 in Fig. 5), which increased in the positive direction exponentially (Fig. 5(c, d)) until eventually delamination (critical damage) occurred (pulse 47 for HfO_2 and pulse 28 for ZrO_2 in Fig. 5) and caused sudden loss of relative transmittance as well as negative phase shift due to material removal. Subsequent laser pulses caused propagation of critical damage along

Optics EXPRESS

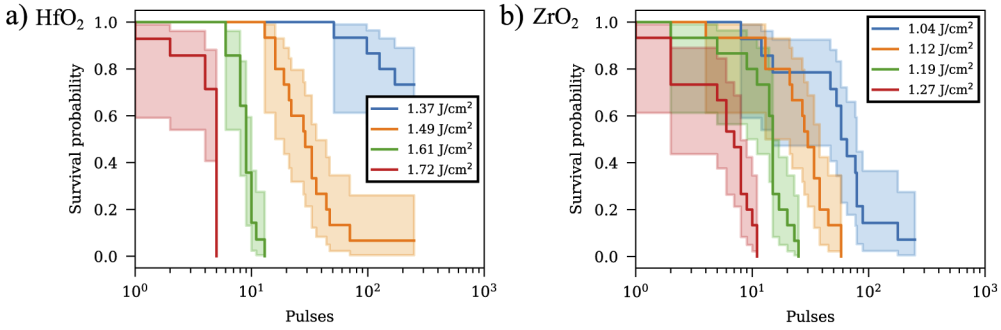

Fig. 4. Survival functions obtained using Kaplan–Meier estimator at four fluence levels for each coating (dashed and dotted lines in Fig. 3): (a) – HfO_2, (b) – ZrO_2.

the beam propagation direction. In the context of this paper, subcritical damage is defined as any changes in the coating that causes it to lose some of its properties (*e.g.* phase retardation) but not macroscopic structural integrity (*e.g.* delamination).

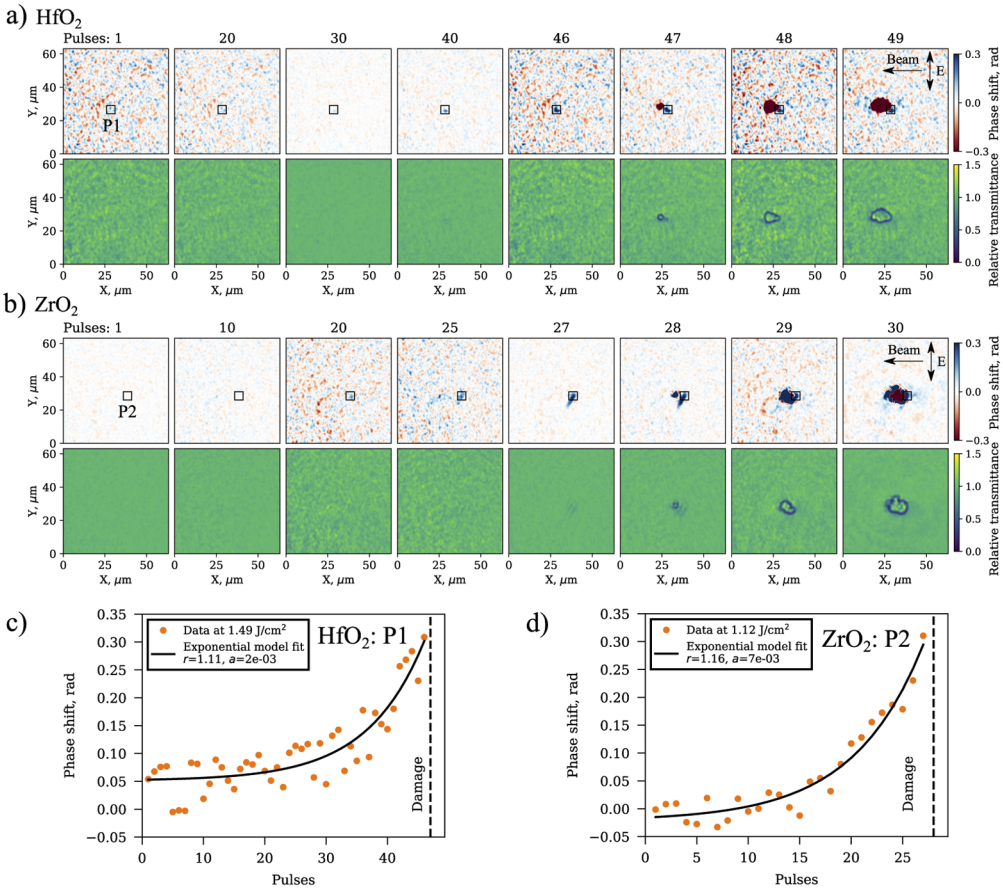

Fig. 5. Example of typical phase shift and relative transmittance data at 1 s probe delay for a single TRDHM test site: (a, b) – selected phase shift and relative transmittance images for HfO_2 and ZrO_2 respectively, (c, d) – phase shift averaged in 5 x 5 μm P1 and P2 regions marked as squares in (a) and (b).

Optics EXPRESS

Phase shift evolution signals (analogous to (c) and (d) in Fig. 5) for all damaged test sites are provided in Fig. 6. The observed positive phase shift during repeated irradiation is believed to be caused by laser-induced defect formation [16] or lattice compaction due to the release of excess energy in molecular bonds [17]. Both of these mechanisms were previously shown to be proportional to irradiation dose and would be seen as positive phase shift in TRDHM experiments. It can also be observed that the median amount of phase shift before critical damage (horizontal lines in Fig. 6) is inversely proportional to irradiation fluence. Previous fluorescence measurements have shown that at high fluence values damage is reached before significant amount of laser-induced defects is generated, while irradiation at lower fluences causes accumulation of more laser-induced defects before damage event occurs [16]. Such observation might be caused by lower trapping efficiencies at higher fluence values or by other mechanisms that cause damage at higher intensities before significant number of defects is induced, however further studies are needed to fully understand this effect.

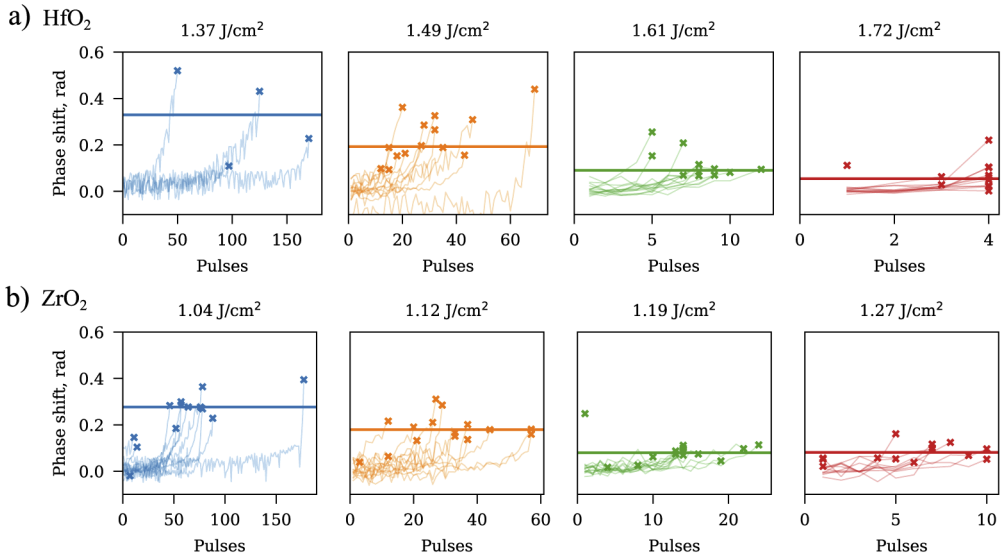

Fig. 6. Phase shift at 1 s probe delay averaged in 5 x 5 μm region for damaged sites at all tested fluences: (a) – HfO_2, (b) – ZrO_2. Horizontal lines indicate median phase shift for each fluence.

3.3. *Morphology of subcritical damage*

Typical morphology of subcritical damage is provided in Fig. 7. From optical microscopy Nomarski images it is evident, that subcritical damage originates at localized absorption centers. Higher resolution AFM images shows that the localized subcritical damage sites on the surface of both HfO_2 and ZrO_2 single layer-coatings are made from nanogrooves featuring a width of around 100 nm. The subcritical nanogrooves are, as expected, oriented perpendicular to irradiation polarization [2,18]. In our experiment nanogrooves reached a length of around 1–2 μm before critical damage occurred. It is interesting to note that other authors have observed growth of nanogrooves to tens of micrometers without reaching critical damage at lower fluences and higher pulse numbers [2,18]. Experimental results suggest that damage process has three distinct stages:

1. Initiation – subsequent laser pulses induce localized incubation, i.e. accumulation of native or laser-induced defect states, which provide seed electrons for nonlinear ionization for subsequent laser pulses [19]. Material compaction due to excess energy stored in the

Optics EXPRESS

bridging bonds can also occur [17]. Localization may be caused by inhomogeneity of the coating or substrate material [10] (some parts of the material are weaker than the others) or by scattering from the rough surface [20,21] (some parts of the coating experience higher intensity than others). Initiation stage corresponds to positive phase shift in regions P1 and P2 in Fig. 5.

2. Subcritical damage – when local electron density reaches a critical value (i.e. when defect states provide enough seed electrons), transparent solid is converted to plasma which results in formation of nanovoids (10–1000 nm) which were observed in both bulk materials (volume and surface) [7,22] and coatings [11]. Local electric field modification around surface nanovoids leads to polarization-dependent nanoablation (perpendicular to polarization in the case of linear polarization) [2,7,18,23]. It was shown that growth of a single nanogroove is linear with pulse count at fluences much lower than 1-on-1 LIDT [18]. Nanovoids and nanogrooves induced by multiple laser pulses can cause phase retardation [24], which was observed *in situ* with TRDHM experiments in this study. Even though subcritical damage stage is visible in AFM images provided in Fig. 7(d) and (h), our experimental setup was not able to distinguish this stage from the initiation stage and to determine its exact threshold.

3. Critical damage – when density of subcritical damages reaches a critical point, delamination of the coating followed by rapid damage crater growth occurs. Delamination can occur due to mechanical failure because of high density of subcritical damage [11], or due to ablation, caused by high intensity regions due to scattering from subcritical damage [25]. This stage corresponds to large areas of negative phase shift in Fig. 5(a) and (b).

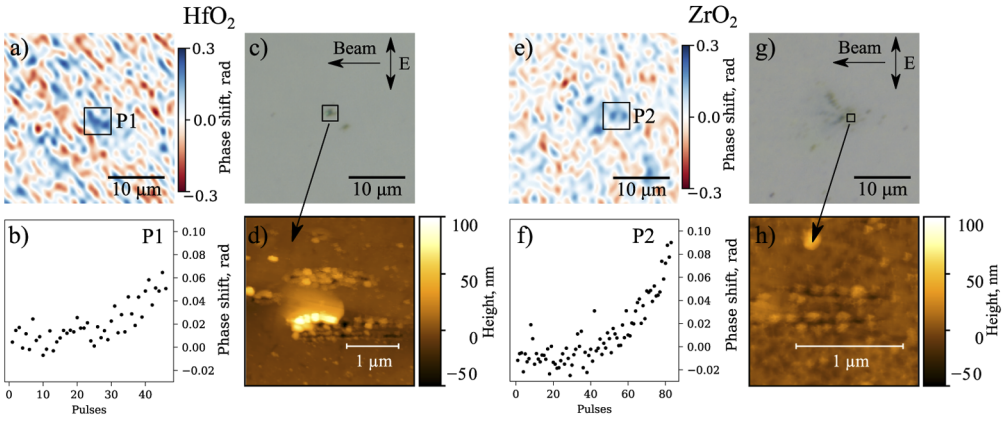

Fig. 7. Typical morphology of subcritical damage for HfO_2 and ZrO_2: (a, e) – phase shift images after irradiation, (b, f) – phase shift averaged in regions P1 and P2 for all pulses used for irradiation, (c, g) – Nomarski microscope images for the same regions as phase shift images (a, e), (d, h) – AFM images for square regions in Nomarski images (c, g).

Similar process was observed in materials like fused silica [7], silicon carbide [26], single- [11,18] and multi-[27] layer dielectric coatings.

3.4. Numerical fatigue model

In order to simulate characteristic S-on-1 damage fatigue curves using data from TRDHM experiment, a stochastic numerical LIDT experiment was constructed. Individual test sites were simulated having randomly distributed defects. Number of defects in each site was determined

Optics EXPRESS

by Poisson distribution given defect density N and site area. Since phase shift incubation is exponential (see Fig. 5(c, d)), phase shift $\Delta\phi_{n,i}$ of a single defect i (at position r_i while peak intensity is I_0) after n laser pulses is:

$$\Delta\phi_{n,i}(I_0, r_i) = \Delta\phi_{1,i}(I_0, r_i)R_i^{n-1}(I_0, r_i), \tag{1}$$

where $\Delta\phi_{1,i}$ – phase shift after first pulse and R_i – growth (incubation) rate. We assume that $\Delta\phi_{1,i}$ is proportional to the amount of free electrons generated during the pulse. For irradiation conditions of the S-on-1 experiment, this number is proportional to multiphoton ionization rate (MPI) [13], therefore:

$$\Delta\phi_{1,i}(I_0, r_i) = \sigma I_i^m(I_0, r_i), \tag{2}$$

where σ is proportionality constant, I_i – local intensity at position r_i and m – order of multiphoton ionization (m = 5 for both HfO_2 and ZrO_2 at 1030 nm). We assume Gaussian beam profile with peak intensity I_0 and beam diameter ω_0:

$$I_i(I_0, r_i) = I_0 \exp\left(-2\frac{r_i^2}{\omega_0^2}\right) \tag{3}$$

Phase shift incubation growth rate R and critical phase shift $\Delta\phi_c$ are intensity dependent and can be determined by fitting experimental TRDHM phase shift data. Model similar in nature to crack growth models used for simulating mechanical fatigue crack growth from cyclic loads [28] was used for incubation growth rate (Fig. 8(b)):

$$R_i = \begin{cases} 1 & : I_i \le I_{th,\infty} \\ \alpha I_i^{\beta}\left(1 - \frac{I_{th,\infty}}{I_i}\right)^{\gamma} + 1 & : I_{th,\infty} < I_i < I_{th,1} \\ \infty & : I_i \ge I_{th,1} \end{cases} \tag{4}$$

where α, β, γ are fit parameters, $I_{th,1}$ – LIDT for a single laser pulse, $I_{th,\infty}$ – LIDT for infinite amount of pulses. Common assumption of crack growth model (verified experimentally [28,29]) which we adopt is that there exists a threshold (in this case $I_{th,\infty}$) below which incubation does not occur (R is equal to 1). In the region $I_{th,\infty} < I_i < I_{th,1}$ growth rate follows a power law function. R is infinite at intensities above $I_{th,1}$, because direct coating ablation becomes the dominant catastrophic damage mode and screens the simulated fatigue mode. This simplified model was chosen because it explains why we observe catastrophic damage when nanogrooves are only 1-2 μm in length, while other authors have observed similar nanogrooves of around few tenths of micrometers in length at lower fluences and larger numbers of pulses without catastrophic damage [2,18].

Table 1. Fatigue model parameters for for HfO_2 and ZrO_2.

	$\Delta\phi_1$		R			$\Delta\phi_c$	
	σ	m	α	β	γ	η	θ
HfO_2	$2 \cdot 10^{-4}$	5	0.0018	13.1	0.2	10	−10
$ZrO2_2$	$4 \cdot 10^{-4}$	5	0.12	9.8	0.7	0.45	−10

A simple power law equation was used for critical phase shift $\Delta\phi_c$ with fit parameters η and θ (Fig. 8(c)):

$$\Delta\phi_c(I_0) = \eta I_0^{\theta}, \tag{5}$$

Critical damage for I_0 after n laser pulses occurs if total phase shift $\Delta\phi_n$ becomes larger than critical phase shift $\Delta\phi_c$:

$$\Delta\phi_n(I_0) = \sum_i \Delta\phi_{n,i}(I_0, r_i), \tag{6}$$

Optics EXPRESS

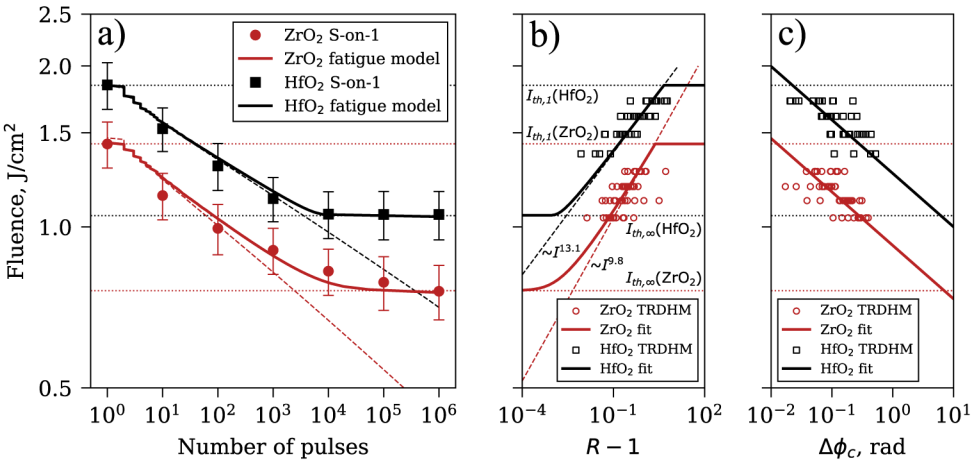

Fig. 8. Proposed fatigue model for HfO_2 and ZrO_2 S-on-1 catastrophic damage curves (a) along with TRDHM data and fits for phase shift incubation growth rate R (b) and critical phase shift $\Delta\phi_c$ (c) (Eqs. (4) and (5) respectively). Fit parameters are provided in Table 1. Dashed lines in (a) and (b) represent fatigue model where growth rate R would be proportional to intensity over the whole range.

$$\Delta\phi_n(I_0) \geq \Delta\phi_c(I_0), \tag{7}$$

Simulated S-on-1 characteristic damage curves (parameters in Table 1) for HfO_2 and ZrO_2 are provided in Fig. 8(a) and are in good agreement with experimental data. It is important to reiterate that most of the parameters were determined directly from TRDHM data (Fig. 8(b) and (c)). Only σ (proportionality constant) and γ (determines curvature in the $I_{th,\infty}$ region) were adjusted to satisfy S-on-1 LIDT data constraints. Surface defect density parameter had no effect on LIDT, however $N = 4 \cdot 10^6$ cm^{-2} was the best value for surface defect density to qualitatively reproduce variance of damaged sites at single intensity level for both HfO_2 and ZrO_2.

HfO_2 and ZrO_2 exhibited different nonlinear growth rates for incubation of subcritical damage ($\sim I^{13.1}$ and $\sim I^{9.8}$ respectively) however the nature of this difference is not yet understood considering that coatings have similar band-gaps and density of localized subcritical damage appears to be both qualitatively and quantitatively similar.

4. Conclusions

LIDT fatigue effect of HfO_2 and ZrO_2 single layer IBS coatings was investigated in femtosecond regime. S-on-1 test confirmed existence of fatigue effect for catastrophic damage in these materials: 10^6-on-1 LIDT decreased to only 57% and 53% of 1-on-1 LIDT for HfO_2 and ZrO_2 respectively. Digital holographic microscopy was used to identify incubation of subcritical damage (increase in optical path length visible as positive phase shift), which preceded critical damage (ablation). Quantitative phase shift data from TRDHM experiments showed that this incubation is exponential in nature and that growth rate of this exponential process and critical phase shift, at which catastrophic damage occurs, are nonlinear functions of irradiation fluence. AFM microscopy was used to show that subcritical damage is made up of localized nanogrooves (100 nm wide, 1–2 μm long) oriented perpendicularly to laser polarization.

A link was established between LIDT fatigue and mechanical fatigue crack growth from cyclic loads which allowed construction of a fatigue model constrained by both S-on-1 and TRDHM experimental data. It was shown that incubation growth rate (as well as incubation threshold) is a nonlinear function of fluence and the proposed model predicts that it should deviate from power

Optics EXPRESS

law function when fluence approaches fatigue limit. These novel findings should be taken into account when extrapolating LIDT fatigue.

Further studies are needed to investigate subcritical damage growth at fluences closer to fatigue limit as well as to explain the differences seen in incubation growth rate for different coatings. More interdisciplinary work is also needed to incorporate well established mechanical fatigue analysis techniques into the field of LIDT research.

Funding

European Regional Development Fund (01.2.2-LMT-K-718-01-0014).

Acknowledgments

The authors would like to thank Simonas Kičas for providing HfO_2 and ZrO_2 IBS coatings along with Tomas Tolenis and Lukas Ramalis for access and help with atomic force microscopy (Center for Physical Sciences and Technology, Vilnius). The authors would also like to thank Lidaris Ltd. for access to motorized differential interference contrast microscope.

Disclosures

The authors declare no conflicts of interest.

References

1. A. E. Chmel, "Fatigue laser-induced damage in transparent materials," Mater. Sci. Eng., B **49**(3), 175–190 (1997).
2. P. K. Velpula, M. Ďurák, D. Kramer, A. R. Meadows, M. Vilémová, and B. Rus, "Evolution of femtosecond laser damage in a hafnia–silica multi-layer dielectric coating," Opt. Lett. **44**(21), 5342–5345 (2019).
3. "ISO 21254-2:2011 Lasers and laser-related equipment – Test methods for laser-induced damage threshold – Part 2: Threshold determination," Standard, International Organization for Standardization, Geneva, Switzerland (2011).
4. D.-B. L. Douti, L. Gallais, and M. Commandré, "Laser-induced damage of optical thin films submitted to 343, 515, and 1030 nm multiple subpicosecond pulses," Opt. Eng. **53**(12), 122509 (2014).
5. S. Guizard, P. Martin, G. Petite, P. D'Oliveira, and P. Meynadieri, "Time-resolved study of laser-induced colour centres in SiO2," J. Phys.: Condens. Matter **8**(9), 1281–1290 (1996).
6. M. Mero, B. R. Clapp, J. C. Jasapara, W. G. Rudolph, D. Ristau, K. Starke, J. Krüger, S. Martin, and W. Kautek, "On the damage behavior of dielectric films when illuminated with multiple femtosecond laser pulses," Opt. Eng. **44**(5), 051107 (2005).
7. F. Liang, R. Vallée, and S. Leang Chin, "Physical evolution of nanograting inscription on the surface of fused silica," Opt. Mater. Express **2**(7), 900–906 (2012).
8. M. Mero, A. J. Sabbah, J. Zeller, and W. Rudolph, "Femtosecond dynamics of dielectric films in the pre-ablation regime," Appl. Phys. A: Mater. Sci. Process. **81**(2), 317–324 (2005).
9. N. Šiaulys, L. Gallais, and A. Melninkaitis, "Direct holographic imaging of ultrafast laser damage process in thin films," Opt. Lett. **39**(7), 2164–2167 (2014).
10. A. Melninkaitis, N. Šiaulys, L. Smalakys, B. Momgaudis, J. Vaicenavičius, S. Barkauskaitė, V. Sirutkaitis, L. Gallais, and S. Guizard, "What time-resolved measurements tell us about femtosecond laser damage?" Proc. SPIE **9632**, 96320O (2015).
11. H. Wang, H. Qi, J. Zhao, B. Wang, and J. Shao, "Transition from isolated submicrometer pits to integral ablation of HfO2 and SiO2 films under subpicosecond irradiation," Opt. Commun. **387**, 214–222 (2017).
12. Z. Sun, M. Lenzner, and W. Rudolph, "Generic incubation law for laser damage and ablation thresholds," J. Appl. Phys. **117**(7), 073102 (2015).
13. L. Smalakys, B. Momgaudis, R. Grigutis, S. Kičas, and A. Melninkaitis, "Contrasted fatigue behavior of laser-induced damage mechanisms in single layer ZrO2 optical coating," Opt. Express **27**(18), 26088–26101 (2019).
14. C. J. Stolz, D. Ristau, M. Turowski, and H. Blaschke, "Thin film femtosecond laser damage competition," Proc. SPIE **7504**, 75040S (2009).
15. E. L. Kaplan and P. Meier, "Nonparametric estimation from incomplete observations," J. Am. Stat. Assoc. **53**(282), 457–481 (1958).
16. A. Beaudier, F. R. Wagner, and J. Y. Natoli, "Using NBOHC fluorescence to predict multi-pulse laser-induced damage in fused silica," Opt. Commun. **402**, 535–539 (2017).
17. F. Piao and W. G. Oldham, "The mechanism of ionization radiation-induced compaction in fused silica," Proc. SPIE **6403**, 640320 (2006).
18. M. Rasedujjaman and L. Gallais, "Polarization dependent laser damage growth of optical coatings at sub-picosecond regime," Opt. Express **26**(19), 24444–24460 (2018).

Optics EXPRESS

19. L. A. Emmert, M. Mero, and W. Rudolph, "Modeling the effect of native and laser-induced states on the dielectric breakdown of wide band gap optical materials by multiple subpicosecond laser pulses," J. Appl. Phys. **108**(4), 043523 (2010).
20. J. Sipe, J. Young, J. Preston, and H. V. Driel, "Laser-induced periodic surface structure. I. Theory," Phys. Rev. B **27**(2), 1141–1154 (1983).
21. J. Sipe, J. Young, J. Preston, and H. V. Driel, "Laser-induced periodic surface structure. II. Experiments on Ge, Si, Al, and brass," Phys. Rev. B **27**(2), 1141–1154 (1983).
22. E. G. Gamaly, S. Juodkazis, K. Nishimura, H. Misawa, B. Luther-Davies, L. Hallo, P. Nicolai, and V. T. Tikhonchuk, "Laser-matter interaction in the bulk of a transparent solid: Confined microexplosion and void formation," Phys. Rev. B: Condens. Matter Mater. Phys. **73**(21), 214101 (2006).
23. A. Rudenko, C. Mauclair, F. Garrelie, R. Stoian, and J. P. Colombier, "Light absorption by surface nanoholes and nanobumps," Appl. Surf. Sci. **470**, 228–233 (2019).
24. A. Čerkauskaite, R. Drevinskas, A. O. Rybaltovskii, and P. G. Kazansky, "Ultrafast laser-induced birefringence in various porosity silica glasses: from fused silica to aerogel," Opt. Express **25**(7), 8011–8021 (2017).
25. M. Sozet, S. Bouillet, J. Berthelot, J. Neauport, L. Lamaignère, and L. Gallais, "Sub-picosecond laser damage growth on high reflective coatings for high power applications," Opt. Express **25**(21), 25767–25781 (2017).
26. H. Shimizu, S. Yada, G. Obara, and M. Terakawa, "Contribution of defect on early stage of LIPSS formation," Opt. Express **22**(15), 17990–17998 (2014).
27. M. Ďurák, P. K. Velpula, D. Kramer, J. Cupal, T. Medrík, J. Hrebícek, J. Golasowski, D. Peceli, M. Kozlová, and B. Rus, "Laser-induced damage threshold tests of ultrafast multilayer dielectric coatings in various environmental conditions relevant for operation of ELI beamlines laser systems," Opt. Eng. **56**, 011024 (2016).
28. F. Fomin, M. Horstmann, N. Huber, and N. Kashaev, "Probabilistic fatigue-life assessment model for laser-welded Ti-6Al-4V butt joints in the high-cycle fatigue regime," Int. J. Fatigue **116**, 22–35 (2018).
29. J. S. Aaldenberg and P. J. Lezzi, "Measurement of the silica glass fatigue limit," J. Am. Ceram. Soc. **103**(5), 3097–3103 (2020).